

LOW VELOCITY IMPACT BEHAVIOR OF THERMOPLASTIC GLASS FIBER COMPOSITES STRENGTHEN WITH STAINLESS STEEL MESH LAYERS

Sepanta Mandegarian¹, Mehdi Hojjati²

¹ Concordia University, Department of Mechanical, Industrial and Aerospace Engineering, Montreal, Quebec, Canada, Ph.D. Candidate, sepanta.mandegarian@concordia.ca

² Concordia University, Department of Mechanical, Industrial and Aerospace Engineering, Montreal, Quebec, Canada, Full Professor, mehdi.hojjati@concordia.ca

Keywords: Low velocity impact, Thermoplastic-based composites, Hybrid laminates, Metal mesh

ABSTRACT

Because of their elastoplastic behavior, metals are capable of absorbing relatively high impact energies. Hybridization also proved to be an advantageous method while composite structures are subjected to impact loading. In the present study, Low Velocity Impact (LVI) response of thermoplastic glass fiber Polypropylene composite laminates strengthening with stainless steel mesh is investigated. It is shown that the hybridized composite laminates could outperform the plain ones under the same LVI energies. Furthermore, the perforation energy is significantly improved compared to the non-hybrid composites manufactured with laminates of the same fiber volume fraction. Eventually, evaluation of the damage extent revealed that the stainless steel mesh layers could change the damage response of the laminates under LVI loading conditions, particularly before the perforation point.

1 INTRODUCTION

Due to their superior mechanical properties to the weight, composite materials become a crucial part of industries such as transportation, renewable energy wind turbine structures, and aerospace. Since these structures are susceptible to impact damages, numerous research is performed to determine the composite response under the Low-Velocity Impact (LVI) loading conditions. These days, hybrid metallic composites are also gaining more attention because of their specific elastoplastic energy absorbing behavior. However, there are very limited attempts examining the hybrid composite laminates strengthen with metal mesh layers. Truong and Choi performed a comprehensive investigation on the tensile behavior of steel wire mesh reinforced composites modifying the mesh size, number of mesh layers, and stacking sequence [1]. In addition to the higher stiffness and ultimate strain of hybrid samples, the laminates with coarse steel wire mesh layers depicted a residual strength after the tensile test. The effect of pressure and fiber direction on the mechanical properties of hybrid composites is assessed, where thermoplastic PPS film is used as both adhesive and filling resin for the mesh layers [2].

LVI test results show that hybrid mesh composite laminates can withstand higher perforation energies compared to non-hybrid samples [3]. Furthermore, the location of the metal mesh plays an important role in the extent of damage and penetration energy. Nonetheless, to the best knowledge of the authors, there is no evaluation of thermoplastic-based composites strengthened with stainless steel mesh under LVI loading conditions. Therefore, the present research focuses on the LVI response of glass fiber laminates strengthen with stainless steel mesh layers.

2 MATERIALS AND TEST PROCESURES

2.1 Fabrication of laminates

2/2 Twill weave Glass/Polypropylene layers with the glass fiber weight fraction of 40% (G^{40}) and 60% (G^{60}), were used to fabricate the composite plates. Stainless steel mesh (M) with the wire diameter of 0.7 mm, opening size of 1.4 mm and mesh size of 12×12 was used to manufacture the hybrid composite laminates. Samples are fabricated using an automated double-belt lamination method in which the dry twill weave layers of Glass/PP laminates and stainless steel mesh are pulled into the oven and pressed together under the constant pressure of the rollers. The layers were heated up to 170°C for 60 seconds in the oven and cooled by air after passing through the press. It is worth mentioning that in order to fill the mesh with thermoplastic resin during the double-belt laminating approach, Glass/PP layers with 40% fiber fraction were used. Finally, three different samples with the stacking sequence of $[G^{40}]_2$, $[G^{60}]_2$, and $[G^{40}/M/G^{40}]$ were manufactured.

2.2 Mechanical properties of the laminates

Quasi-static tensile tests were performed for the laminates and metal mesh separately while following the ASTM D3039 [4] standard to determine the tensile mechanical properties. Using a diamond saw machine, specimens were cut in the fiber direction with the dimensions of 250 mm × 25 mm and proper tabs were attached to samples with the epoxy adhesive DP 460. It is worth noting that in order to run the tensile tests for the mesh samples, only 12 stainless steel wires are positioned in the tensile direction. All the tensile tests were carried out using an MTS universal test machine equipped with a 100 kN load cell under the standard test rate of 2mm/min. The tests were repeated three times for each lamination. Finally, the measured mechanical properties of composite samples and stainless steel mesh are presented in Table 1.

Stacking sequence	$[G^{40}]_2$	$[G^{60}]_2$	$[G^{40}/M/G^{40}]$	Stainless steel mesh
Plate thickness (mm)	1.96	2.26	2.35	1.4
Tensile strength (MPa)	174.0	230.7	125.1	747.9
Tensile modulus (GPa)	8.4	12.9	8.1	83.17
Maximum force (kN)	7.54	12.32	7.30	3.45
Ultimate strain (%)	2.49	2.16	1.98	0.17

Table 1: Mechanical properties of composite plates and stainless steel mesh

As Hasselbruch et al. depicted, linear elastic, non-linear plastic deformation, and finally stepwise consecutive failure of wires occur for stainless steel mesh under quasi-static tensile loading [2]. Similar results were accomplished for the metal mesh samples under tension loading. The tensile strength of samples with stainless steel mesh layers is lower compared to non-hybrid ones, which could be the consequence of imperfect bonding between the metal mesh and glass/PP layers. These improperly bonded locations could cause stress concentration and accelerate the final failure. Nevertheless, the tensile modulus and maximum bearable force of the hybrid $[G^{40}/M/G^{40}]$ sample and $[G^{40}]_2$ are almost the same. Yet, it is worth mentioning that some of the hybrid samples did not separate completely in two pieces after the catastrophic failure.

2.3 Impact test procedures

LVI tests are performed using the Instron 3940 drop weight impact machine according to ASTM D7136 [5], instrumented with a 22 kN load cell. Plate samples with the dimension of 100 mm × 150 mm were clamped on an open rectangular fixture of 125 mm × 75 mm by four rubber-headed clamps. 15, 22.5, 26, 30, 35, 40, 45, 50, 60, and 75 J impact tests are done with a 16 mm diameter hemispherical tup

while the velocity is controlled and set around 3.03 m/s to 3.13 m/s. Because the velocity of impactor tup is kept almost constant, the drop weight height also maintained within the close range of 469 mm to 499 mm. Hence, with respect to the mentioned applied impact energies additional weights are required on the impactor tup to obtain the total striker mass range of 3.265 kg to 16.265 kg. It is noteworthy that the samples were only subjected to specific impact energies considering their perforation impact point.

The force-time data was recorded at 2000 kHz sampling frequency using the data acquisition system. The velocity of the impactor before contacting with the sample surface is also measured by the piezoelectric sensor; therefore, by means of collected data, the values for velocity, displacement and energy could be driven at the impact loading [6].

After being hit by the impactor and before removing from the fixture, the permanent indentation depth of the impacted point is measured using a dial gauge indicator with the accuracy of up to ± 0.01 inches. Furthermore, since the damages can change the translucency, the backlight can significantly facilitate damage detection [7]. Thus, to evaluate the extent of damage after impact in addition to the normal side, or top views of the samples, the backlight method is used to take pictures.

3 RESULTS AND DISCUSSION

3.1 Low velocity impact response

Composite laminates under LVI situations could show different behavior which is significantly affected by the applied impact energy, laminate thickness, tup dimensions and etc. [8,9]. Under relatively lower impact energies, the striker would bounce back after hitting the surface, which is known as the rebound condition. During the rebound phenomenon, the applied energy is partially absorbed by the laminate while the rest is given back to the striker resulting in the bounce back of the impactor tup. This bounce back is the elastic response of the laminate to LVI loading while the absorbed energy could be a combination of plastic deformation, damages, and friction. The initiation damage point could be captured by a sudden drop in the force data where the laminate mechanical properties decrease due to either in-plane or out-of-plane damages [6].

Since the mechanical properties of laminated composites such as the tensile properties could substantially vary with the fiber volume fraction, it is expected to obtain better LVI behavior for $[G^{60}]_2$ laminates. As presented in figure 1, the hybrid composite laminates outperform the non-hybrid $[G^{40}]_2$ samples. Under 15 J impact tests both $[G^{60}]_2$, $[G^{40}/M/G^{40}]$ laminates absorb around 50% of the energy showing a rebound situation. However, $[G^{40}]_2$ samples absorb more than 70% of the impacted energy reaching a sudden drop in force before rebounding. Hence, higher scope of damage is anticipated for $[G^{40}]_2$ laminates under LVI loading conditions in a rebound situation.

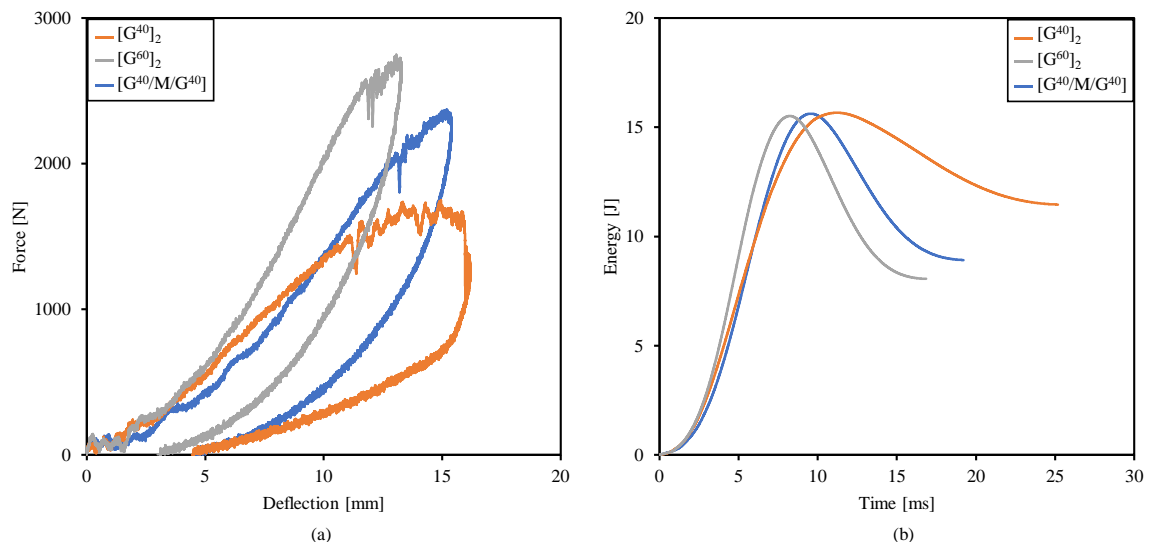


Figure 1. Comparison of LVI response of hybrid and non-hybrid composite laminates under 15 J impact test, (a) force-deflection curve, (b) energy-time diagram

Under higher LVI energies, not only the extent of damage increases, but also the response of impacted laminates could change from rebound to contact or perforation. These variations could be determined with a major drop in load followed by a permanent penetration of the tup head into the laminates; therefore, under a perforation situation, the total applied impact energy should be absorbed by the laminate [6]. Figure 2 (a) shows a sudden drop in the force value for $[G^{40}]_2$ sample indicating a catastrophic failure point and perforating the plate under the 30 J impact test. The energy diagram for this laminate also shows that the impact energy is fully absorbed and caused perforation. Nevertheless, strengthening the laminate with stainless steel mesh improved the impact properties. Hybrid $[G^{40}/M/G^{40}]$ composite laminate almost absorbed the same impact energy as $[G^{60}]_2$ in a rebound behavior under 30 J impact condition. As figure 3 represents, the hybrid laminate perforates under 50 J impact energy. Observations showed that the $[G^{60}]_2$ laminate should fail around the same impact energy (50-60 J). However, because of the high values of plate deformation, the striker tup was blocked by protection dampers which also resulted in an abrupt increase of force before the impactor bounce back. It is worth mentioning that the damage initiation points for hybridized composite laminates occur at higher deflection levels compared to the plain ones.

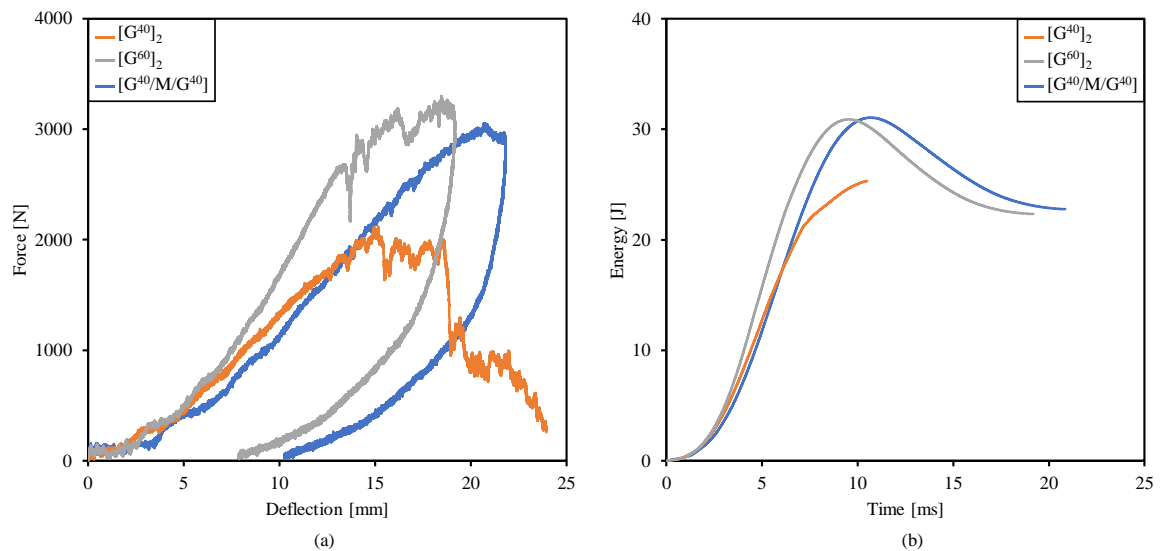


Figure 2. LVI response of hybrid and non-hybrid composite laminates under 30 J impact test, (a) force-deflection curve, (b) energy-time diagram

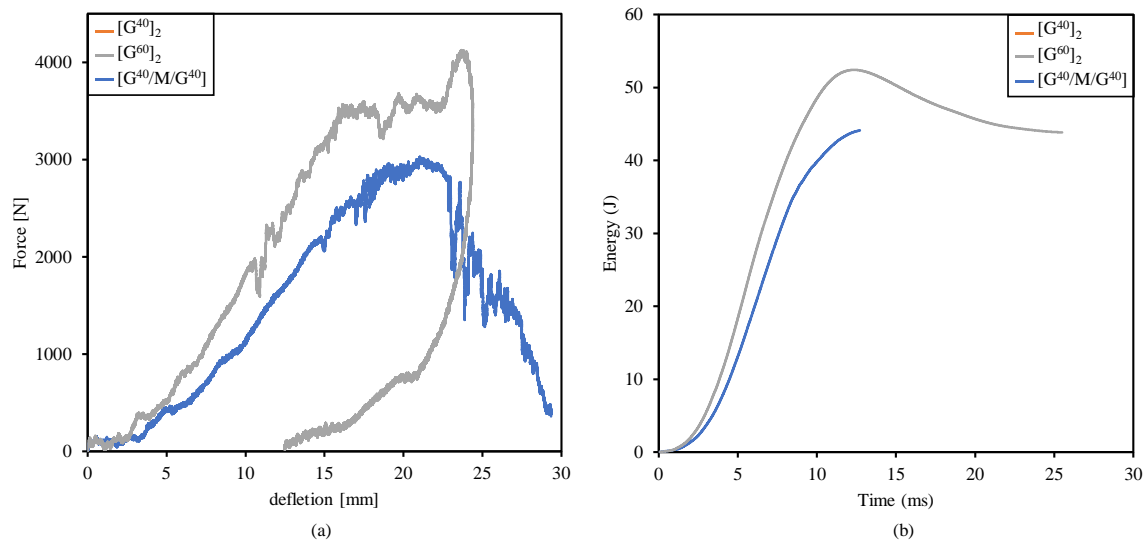


Figure 3. LVI response of $[G^{60}]_2$, $[G^{40}/M/G^{40}]$ laminates under 50 J impact test, (a) force-deflection curve, (b) energy-time diagram

LVI evaluations revealed that in an energy profile diagram, the perforation happens when the absorbed energy equalizes the impact energy. After this point, the energy profile separates downward the diagonal line by entering the perforation state [3,10]. Similar results were accomplished by examining the energy profile as depicted in figure 4, where the absorbed energy considerably withdraws the diagonal line reaching the perforation point. It is revealed that the plain $[G^{40}]_2$ laminates perforate under 30 J impact energy. Nonetheless, strengthening the laminate with stainless steel mesh layer improved the impact perforation resistance to the levels of plain $[G^{60}]_2$ laminates. Moreover, both $[G^{40}/M/G^{40}]$ and $[G^{60}]_2$ laminates exhibit an analogous response in the absorbed energy percentage in the rebound conditions. Yet, the type and extent of damage varies for these composite samples which will be assessed in the following section.

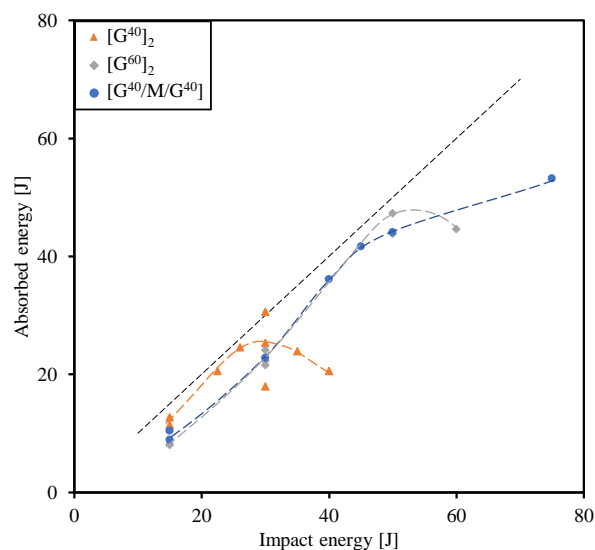


Figure 4. Energy profile of hybrid and non-hybrid composite laminates

3.2 Damage propagation under impact

In addition to the mentioned force-deflection and energy-time graphs, there are several complementary diagrams which could be used to assess the material response under LVI loading. For

instance, figure 5, which depicts the maximum impactor tup displacement during the impact test, could be evaluated as a damage indicator. If the laminate does not perforate under the impact load, the striker reaches the maximum displacement exactly one step before the bounce-back point. The higher the impact energy is, the more the laminate deforms under impact. It is also expected to see a sudden rise in the tup displacement when the laminates are perforated. Nonetheless, following the ASTM D7136 [5] standard for the current thin laminates, the tup is stopped by the machine's dampers when the striker penetrates through the samples. Hence, instead of an expected jump shown by black arrows in figure 5, the tup displacement was controlled by the dampers at a specific level after the perforation. Furthermore, examinations show that the laminates strengthened with stainless steel mesh could sustain higher deformation before penetrating. Lower stiffness of the hybridized glass/PP composites and higher plastic deformation of these laminates could be the reason for the enhanced maximum bearable displacement.

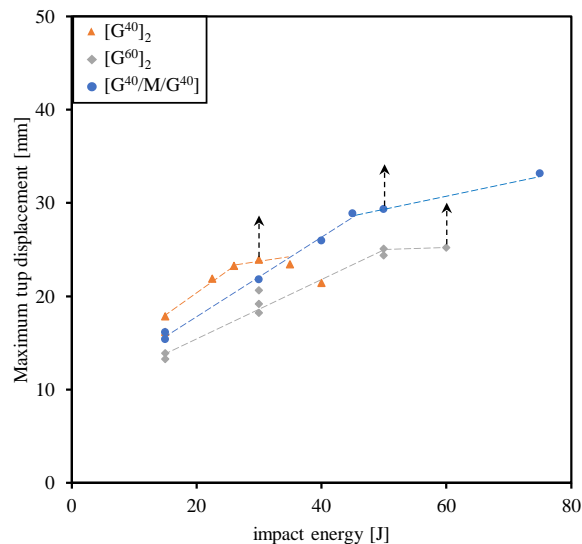


Figure 5. Maximum impactor tup displacement of hybrid and plain laminates during LVI tests

The stiffness of the laminate is susceptible to the damages occurred by the applied impact force; therefore, a combination of damage and plastic deformation causes irreversible deformation under LVI situations. As mentioned in the test procedures, the permanent deformation of the impacted point, which is a representation of damage extent, is measured. Before reaching the perforation point, the permanent deformation of laminates shows a corresponding increase with the amount of impact energy. In figure 6 the rising arrows pinpoint the perforation of laminates. Examination of deformation also proves that strengthening the plain sample with stainless steel mesh improves the material's behavior under impact. [G⁴⁰/M/G⁴⁰] hybrid composite laminates undergo less damage which results in lower permanent deformation compared to the [G⁴⁰]₂ ones. Besides, due to the elastic behavior of the materials, relatively considerable displacement of the hybrid laminates is recovered, returning partial energy required for the tup bounce back.

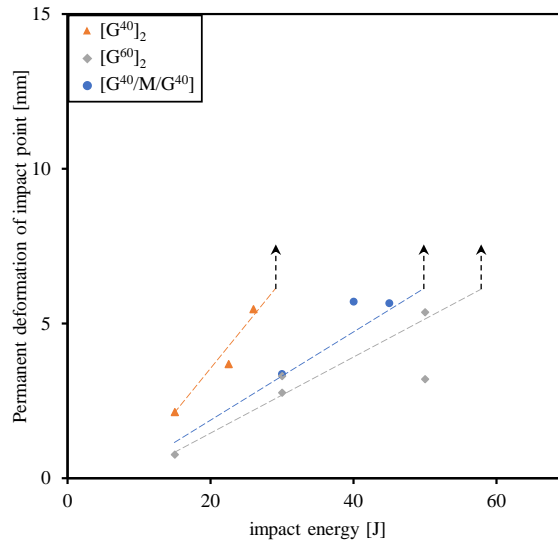


Figure 6. Permanent deformation of hybrid and plain composite laminates after LVI tests

Since the damage affects the transparency of the glass/PP composites, the extent of damage could be determined as darker parts using the backlight source. Figures 7, and 8 provide top and side views of the [G⁴⁰]₂ plain laminate under certain LVI energies. Due to the increase of the applied impact energy, a rise in damaged area is depicted. A combination of matrix cracking and fiber failure is particularly visible at the rear impact side where the laminate is under tensile bending load. Because of the mentioned rise in the extension of impact damage, higher permanent deformation is accomplished as the impact energy grows. Finally, the reversible deformation part before reaching the perforation state is happening due to the elastoplastic behavior of the glass/PP composite laminates.

Because the fiber volume fraction of the plain [G⁶⁰]₂ composites is higher than [G⁴⁰]₂, these samples are expected to be more stiff and higher resistant to the impact load. An evaluation of the damage extent specified by the backlight method also proves the higher resistance of [G⁶⁰]₂ laminate to the LVI loading situation. Moreover, it could be observed in figure 9 that before the perforation state, the extent of damage is directly proportional to the impact energy. For [G⁶⁰]₂ laminates, it is clearer that the initiation of fiber breakage occurs at the tension bending side. Eventually, pictures of the side view sections of the impacted location in figure 10 determine lower irreversible deformation of laminates with the higher fiber volume fraction under LVI conditions.

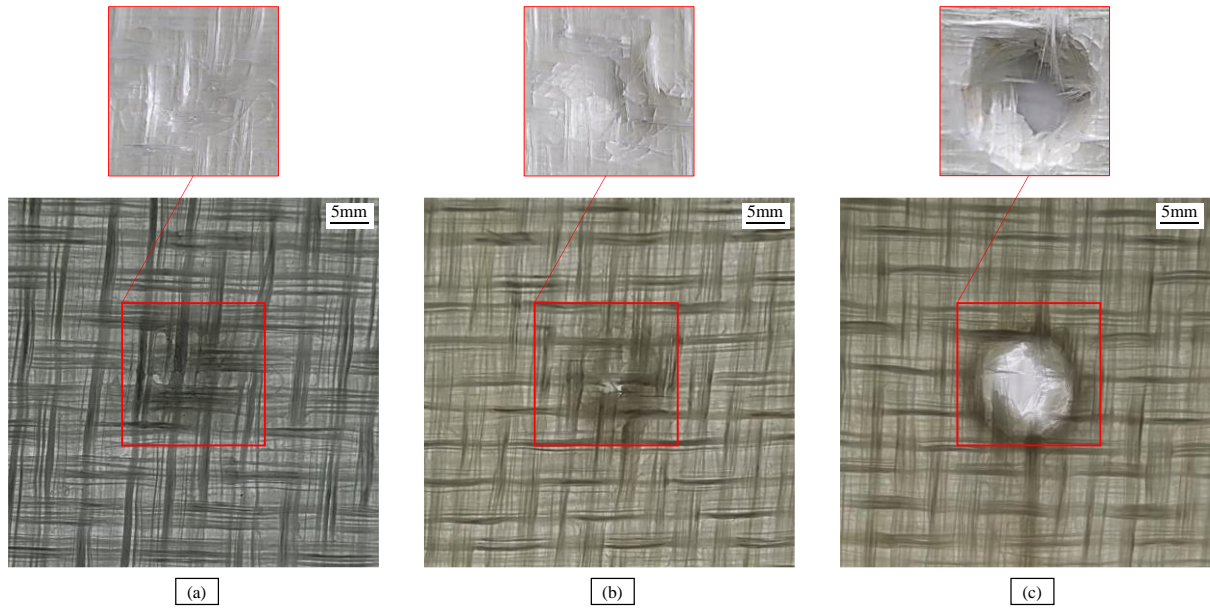


Figure 7. Top view of $[G^{40}]_2$ laminates with and without the backlight source under different impact energies, (a) 15 J, (b) 22.5 J, (c) 30 J



Figure 8. Side view of $[G^{40}]_2$ laminates under various LVI energies, (a) 15 J, (b) 22.5 J, (c) 30 J

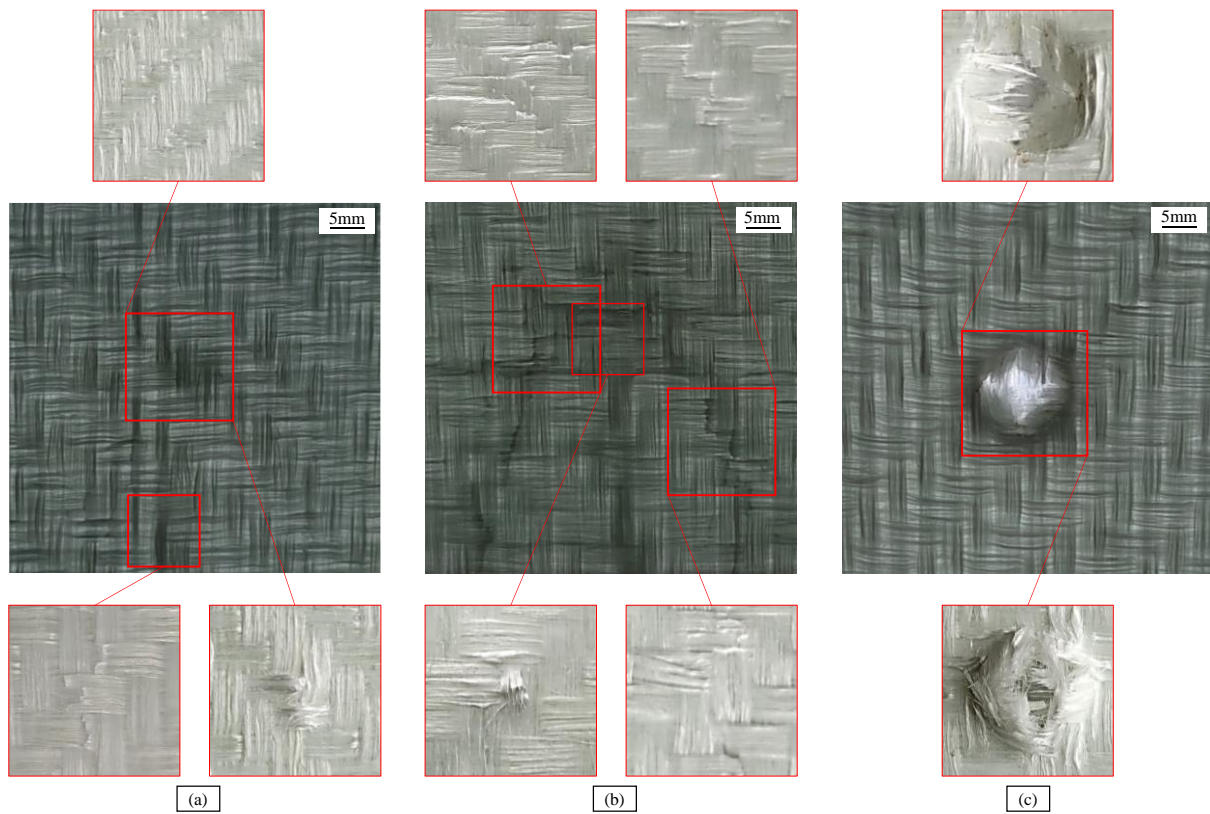


Figure 9. Top and bottom view of $[G^{60}]_2$ laminates with and without the backlight source under different impact energies, (a) 15 J, (b) 30 J, (c) 60 J



Figure 10. Side view of $[G^{60}]_2$ laminates under certain LVI energies, (a) 15 J, (b) 30 J, (c) 60 J

Since the presence of metal mesh significantly affects the transparency of the composite laminates, the backlight method is not quite suitable for these samples. Even though the exact impacted location blurs a little because of the occurred damage, the progression of damage could not be well defined using backlight. In comparison to the plain $[G^{40}]_2$ laminates, hybridized plates undergo less damage under LVI loading. A considerable part of the impact deformation restores due to the elastoplastic response of the laminates strengthened with stainless steel mesh. Furthermore, because of the capability of plastic deformation, these materials are expected to absorb a considerable percentage of the applied impact energy. Hence, as figure 11 confirms, the extent of damage is lower for the $[G^{40}/M/G^{40}]$ hybrid composite laminates compared to the non-hybrid ones. Laminates with embedded stainless steel mesh layers also result in fiber breakage at the rear impact site under LVI.

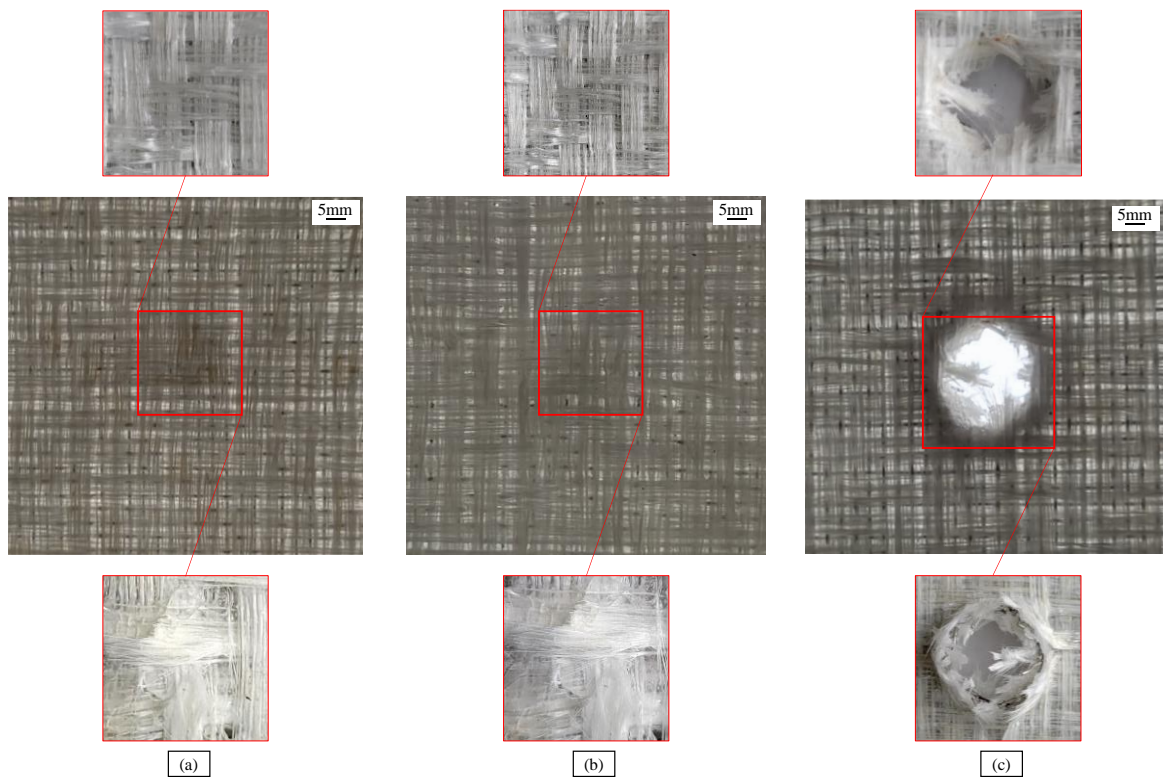


Figure 11. Top and bottom view of $[G^{40}/M/G^{40}]$ hybrid composite laminates with and without the backlight source under different impact energies, (a) 15 J, (b) 30 J, (c) 50 J



Figure 12. Side view of $[G^{40}/M/G^{40}]$ hybrid composite laminates under various impact energies, (a) 15 J, (b) 30 J, (c) 50 J

Containing a higher fiber volume fraction, plain $[G^{60}]_2$ laminates are more stiff than the $[G^{40}/M/G^{40}]$ hybrid ones. In addition to that, laminates strengthened with stainless steel mesh are relatively more deformable because of the plastic response of metals; therefore, as depicted in figure 12 and evaluated in the previous section, the permanent deformation of the hybrid samples is higher compared to the plain $[G^{60}]_2$ laminates. Moreover, delamination between the metal mesh layer and the composites is a more visible damage scenario, especially in the hybrid samples comparing its side view with the $[G^{60}]_2$ samples under the 30 J LVI test.

4 CONCLUSIONS

In the current paper the LVI behaviour of thermoplastic woven composites strengthen with metal mesh was investigate. In addition to the collected data from the impact test machine, the after impact damage extent and deformation of the laminate was evaluated precisely. It is revealed that hybridizing the glass/PP composites with stainless steel mesh improved the LVI response of laminates. Higher impact energies are required to penetrate the $[G^{40}/M/G^{40}]$ hybrid laminates in contrast to the plain $[G^{40}]_2$ ones. The presence of steel mesh positively decreased the after impact damage and permanent deformation. Yet, the results of the energy profile depicts a considerable resemblance between the $[G^{40}/M/G^{40}]$ and $[G^{60}]_2$ composite samples. Although backlight method was not reliable for the hybrid laminates, assessments of the different section views depicted lower damage extent for the laminates strengthen with stainless steel mesh under various LVI energies. Matrix cracks and fiber failure damage was clearly depicted in all the impacted samples, while delamination of metal mesh layers and composites was also noticed under LVI.

5 ACKNOWLEDGEMENTS

Financial support is provided by Natural Sciences and Engineering Research Council of Canada (NSERC), and Innovative Composite Products (ICP) through Alliance program.

6 REFERENCES

- [1] G.T. Truong and K.K. Choi, Tensile behavior of hybrid composites of carbon fibers-steel wire mesh reinforced polymer, *Mechanics of Advanced Materials and Structures*, 28, 2021, pp. 154-156 (doi: [10.1080/15376494.2018.1553256](https://doi.org/10.1080/15376494.2018.1553256)).
- [2] H. Hasselbruch, A. Von Hehl and H.W. Zoch, Properties and failure behavior of hybrid wire mesh/carbon fiber reinforced thermoplastic composites under quasi-static tensile load, *Material and Designs*, 66, 2015, pp. 429-436 (doi: [10.1016/j.matdes.2014.07.032](https://doi.org/10.1016/j.matdes.2014.07.032)).
- [3] T.J. Ahmed, H.E.N. Bersee and A. Beukers, Low velocity impact on woven glass composites reinforced with metal mesh layers, *16th International Conference on Composite Materials (ICCM 16)*, Kyoto Japan, July 8-13, 2007.
- [4] ASTM D3039 / D3039M - 17, *Standard Test Method for Tensile Properties of Polymer Matrix Composite Materials*, ASTM International 2017 (doi: [10.1520/D3039_D3039M-17](https://doi.org/10.1520/D3039_D3039M-17)).
- [5] ASTM D7136 / D7136M – 15, *Standard Test Method for Measuring the Damage Resistance of a Fiber-Reinforced Polymer Matrix Composite to a Drop-Weight Impact Event*, ASTM International 2015 (doi: [10.1520/D7136_D7136M-15](https://doi.org/10.1520/D7136_D7136M-15)).
- [6] S.Z.H. Shah, S. Karuppanan, P.S.M Megat-Yusoff and Z. Sajid, Impact resistance and damage tolerance of fiber reinforced composites: A review, *Composite Structures*, 217, 2019, pp. 100-121 (doi: [10.1016/j.compstruct.2019.03.021](https://doi.org/10.1016/j.compstruct.2019.03.021)).
- [7] S.Z.H. Shah, P.S.M Megat-Yusoff, S. Karuppanan, R.S. Choudhry, F. Ahmad, Z. Sajid , et al. Performance comparison of resin-infused thermoplastic and thermoset 3D fabric composites under impact loading, *International Journal of Mechanical Sciences*, 189, 2021 (doi: [10.1016/j.ijmecsci.2020.105984](https://doi.org/10.1016/j.ijmecsci.2020.105984)).

- [8] G. Caprino and V. Lopresto, On the penetration energy for fibre-reinforced plastics under low-velocity impact conditions, *Composite Science and Technology*, 61, 2001, pp. 65-73 (doi: [10.1016/S0266-3538\(00\)00152-4](https://doi.org/10.1016/S0266-3538(00)00152-4)).
- [9] G. Caprino, A. Langella and V. Lopresto, Indentation and penetration of carbon fibre reinforced plastic laminates. *Composites Part B Engineering*, 34, 2003, pp. 319-325 (doi: [10.1016/S1359-8368\(03\)00002-7](https://doi.org/10.1016/S1359-8368(03)00002-7)).
- [10] C. Atas and D. Liu, Impact response of woven composites with small weaving angles, *International Journal of Impact Engineering*, 35, 2008, pp. 80-97 (doi: [10.1016/j.ijimpeng.2006.12.004](https://doi.org/10.1016/j.ijimpeng.2006.12.004)).